Molecular basis of transport and regulation in the Na+/betaine symporter BetP

Ressl, Susanne; Terwisscha van Scheltinga, Anke C.; Vonrhein, Clemens; Ott, Vera; Ziegler, Christine

Published in:
Nature

DOI:
10.1038/nature07819

Publication date:
2009

SUPPLEMENTARY INFORMATION

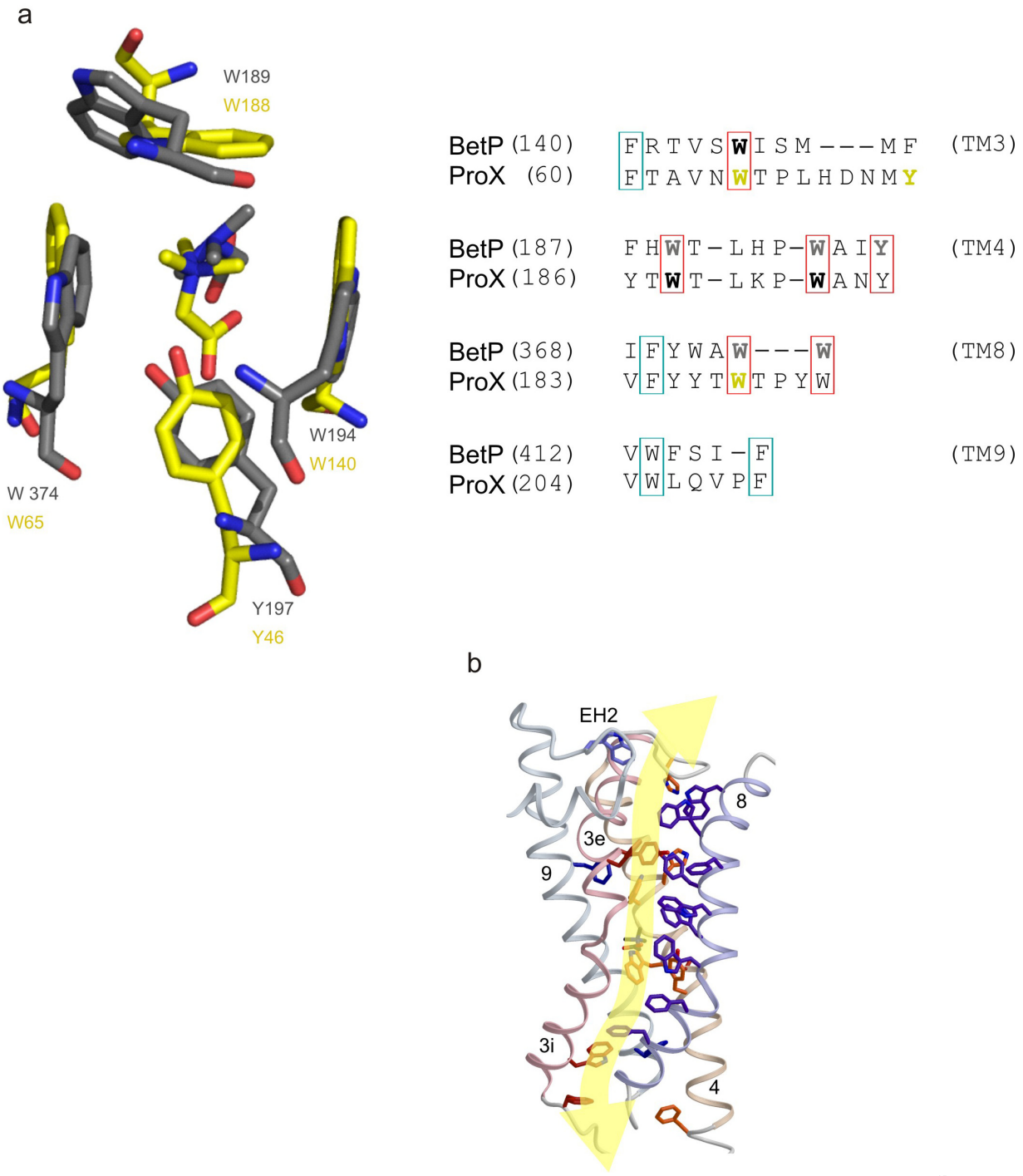

Figure S1: a, Overlay of the glycine betaine binding pocket of BetP (grey) and the periplasmic glycine betaine binding protein ProX[15] from *E. coli* (yellow). Corresponding side chains are labeled with respect to their orientation in the Trp box. **b,** Sequence homology between BetP and ProX in the 4-helix bundle TM3, TM4/TM8, TM9 of BetP. **c,** 23 aromatic side chains in the central 4-helix bundle TM3, TM4/TM8, TM9 line the substrate pathway (light yellow). The assembly of aromatic residues in BCC transporters may be related to the broad spectrum of different osmolytes that can be transported. Assuming that BCC transporters exhibit the same overall fold with a rather narrow substrate pathway, a general solution for osmolyte transport would be to provide several aromatic boxes along the pathway. Clearly, such pathway composition creates surface properties ensuring that a wide variety of osmolytes can be transported without interaction with the protein backbone.

C

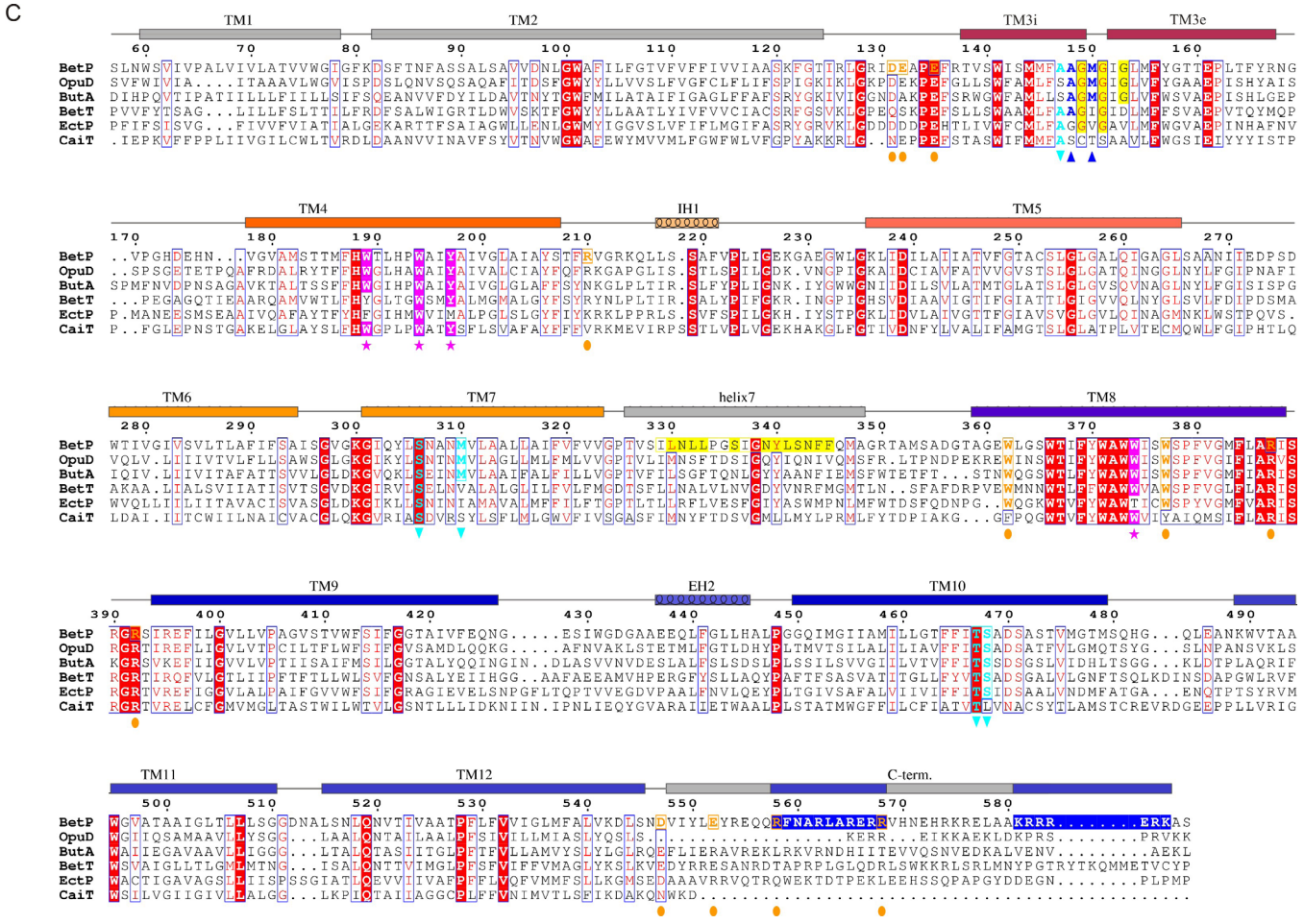

Figure S2: Amino acid sequence alignment of *C. glutamicum* BetP with five transporters of the BCCT family: Na^+/glycine betaine transporter OpuD from *B. subtilis*, Na^+/glycine betaine transporter ButA from *Tetragenococcus halophila*, H^+/choline transporter BetT from *E. coli*, Na^+/ectoine transporter EctP from *C. glutamicum*, and carnitine/γ-butyrobetaine antiporter CaiT from *E. coli* using ClustalW multiple sequence alignment displayed by ESPript 2.2 (http://espript.ibcp.fr/ESPript). Strictly conserved residues are displayed in red. α-helices of the BetP structure are shown as cylinders in top of the BetP sequence. Residues potentially involved in coordinating sodium ions are marked with triangles shown in blue (Na1) or cyan (Na2). The conserved G-x-G-x-G motif of sodium-coupled transporters in the BCCT family in TM3 is yellow. The magenta stars indicate residues involved in glycine betaine-binding. Orange colored residues in TM8 and TM9 show additional substrate-binding sites, residues involved in trimer formation or regulatory interactions are labeled with an orange circle.

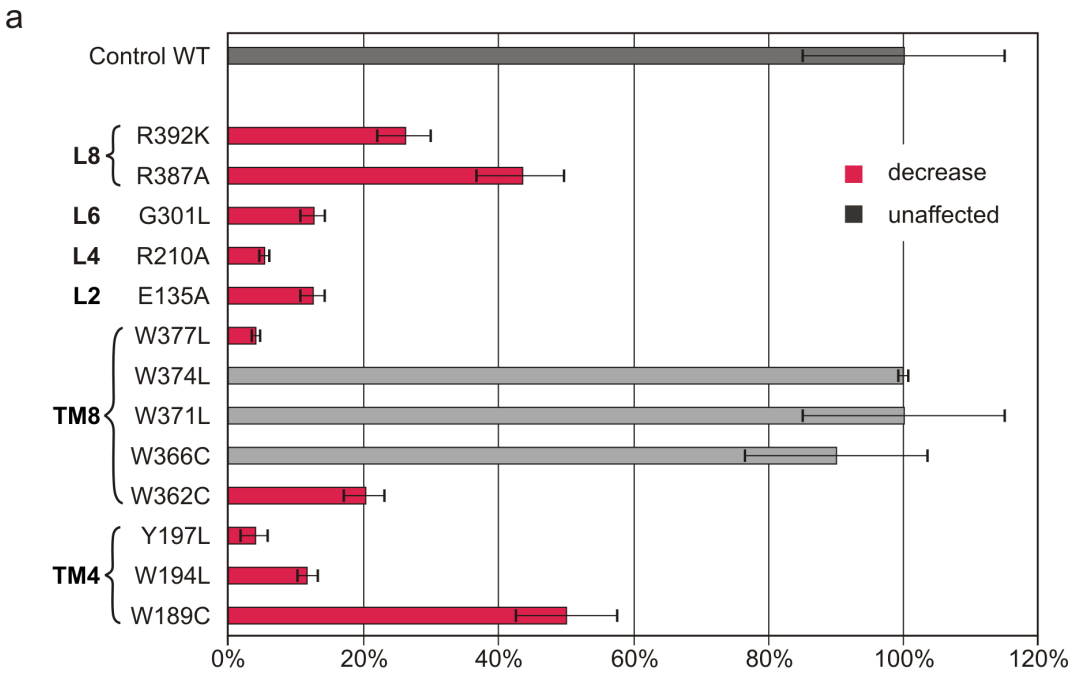

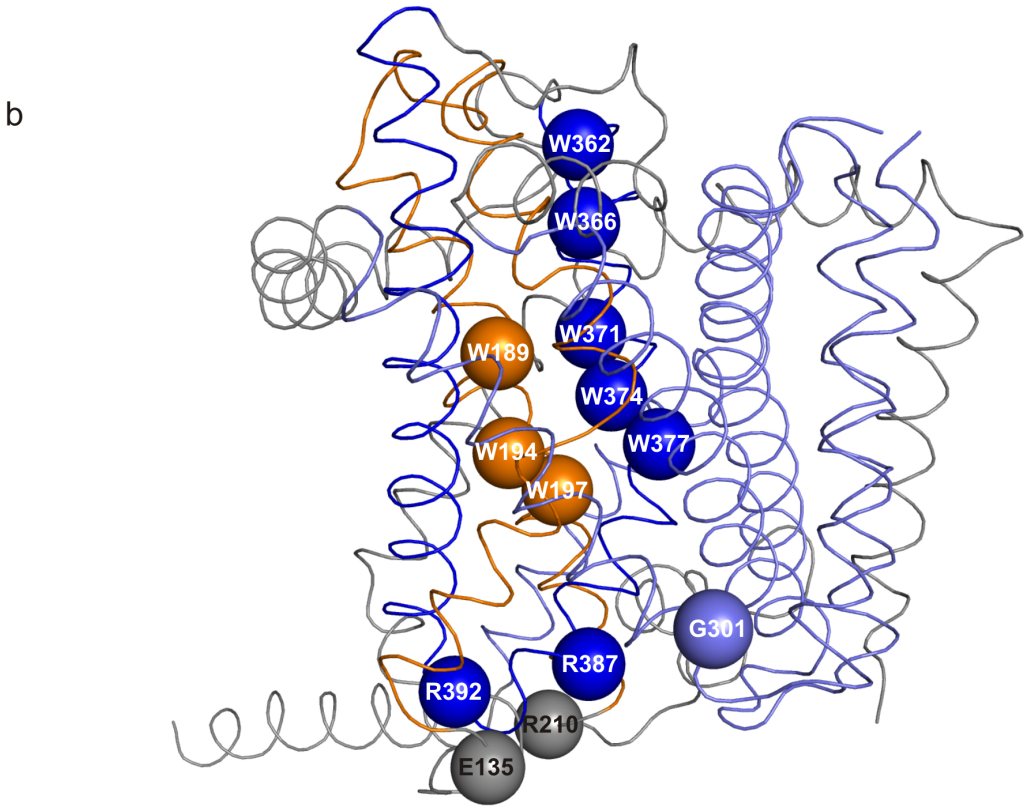

Figure S3: a, Transport activity determined from the initial slopes of [^{14}C]glycine betaine uptake time curves of BetP mutants. Activity is expressed as percentage of WT control (100%) at optimal osmolarity. The expression levels of mutants were assessed by immuno-blotting against the N-terminal StrepII tag and activity was normalized accordingly. **b,** Location of functionally important residues in the BetP monomer.

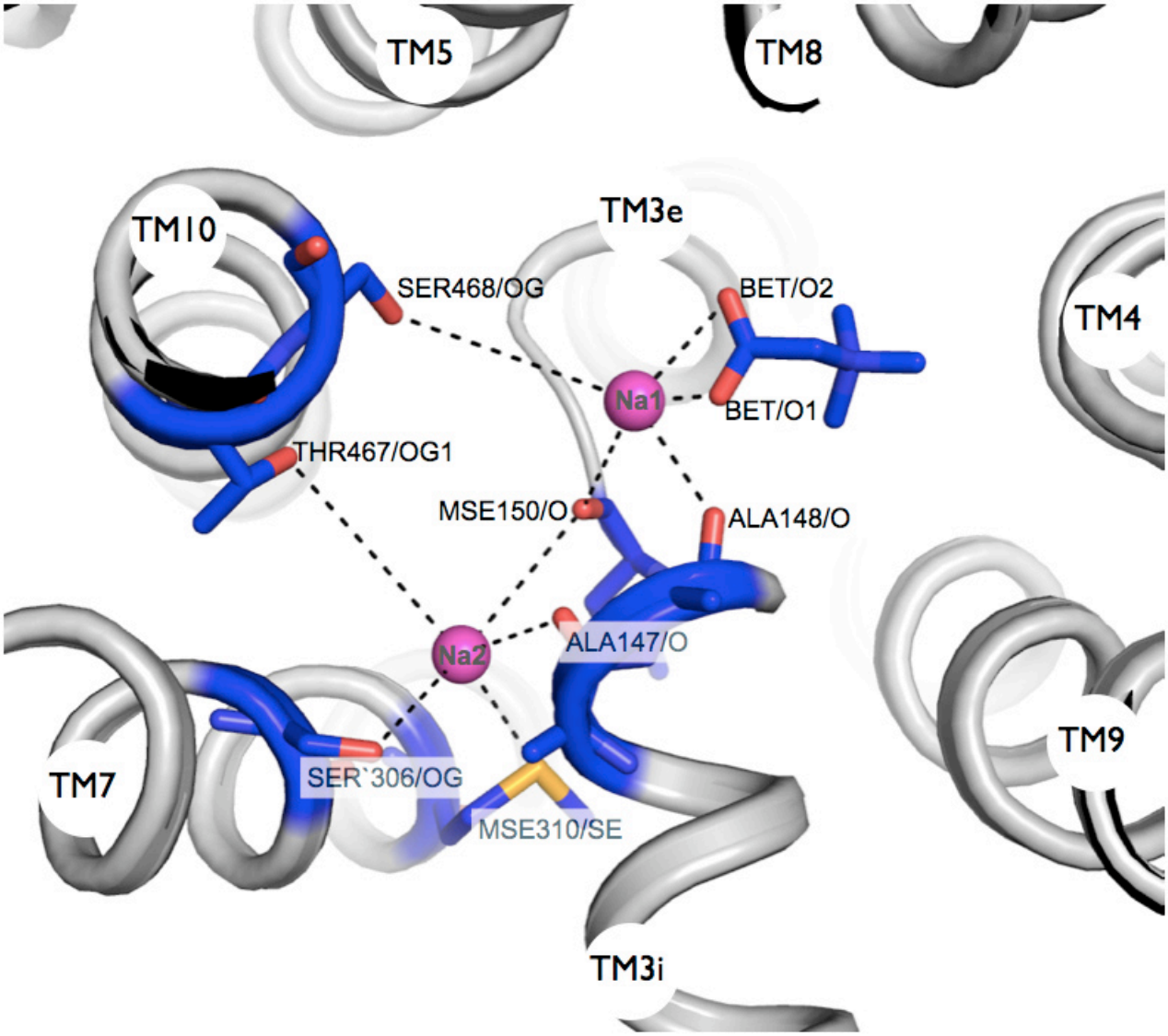

Figure S4: Potential sodium ion binding sites in BetP assigned *via* structural superposition with $LeuT_{Aa}$. View from the cytoplasm with sodium ions in magenta and black dotted lines indicate the coordination between the atoms of residues involved in Na^+ binding. The helices TM3i, TM3e, TM4, TM5, TM7, TM8 and TM10 are displayed in light-grey. The sodium ions were not included in the refinement process.

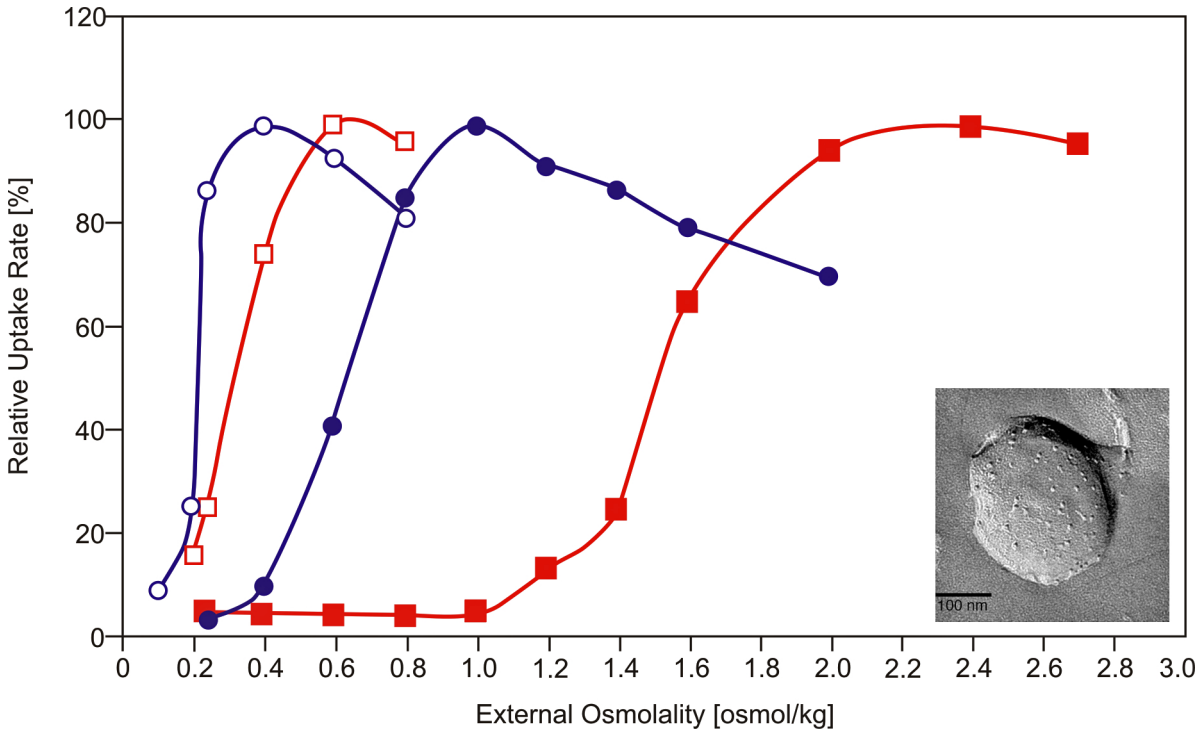

Figure S5: a, Glycine betaine uptake of BetPΔN29 was measured in DHPF *C. glutamicum* cells (■, maximal uptake rate 11 nmol glycine betaine/min mg dry cells) and in *E. coli* polar lipid proteoliposomes (□, 268 nmol glycine betaine/min mg protein) in dependence on the external osmolality adjusted with NaCl (cells) or proline (proteoliposomes) in the external buffer (25 mM KPi, pH 7,5; 100 mM NaCl). BetP WT was measured as a control in DHPF *C. glutamicum cells* (●,100.8 nmol glycine betaine/min mg dry cells) and in *E. coli* polar lipid proteoliposomes (○, 771 nmol glycine betaine/min mg protein). Uptake was started by adding 250 µM [^{14}C]-glycine betaine. Maximum uptake at optimum conditions of external osmolality was taken as 100%. Inset: Micrograph of a freeze fractured proteoliposomes suspension of BetPΔN29 reconstituted into *E. coli* polar lipids at a lipid to protein ratio of 30 to 1 (mol/mol).

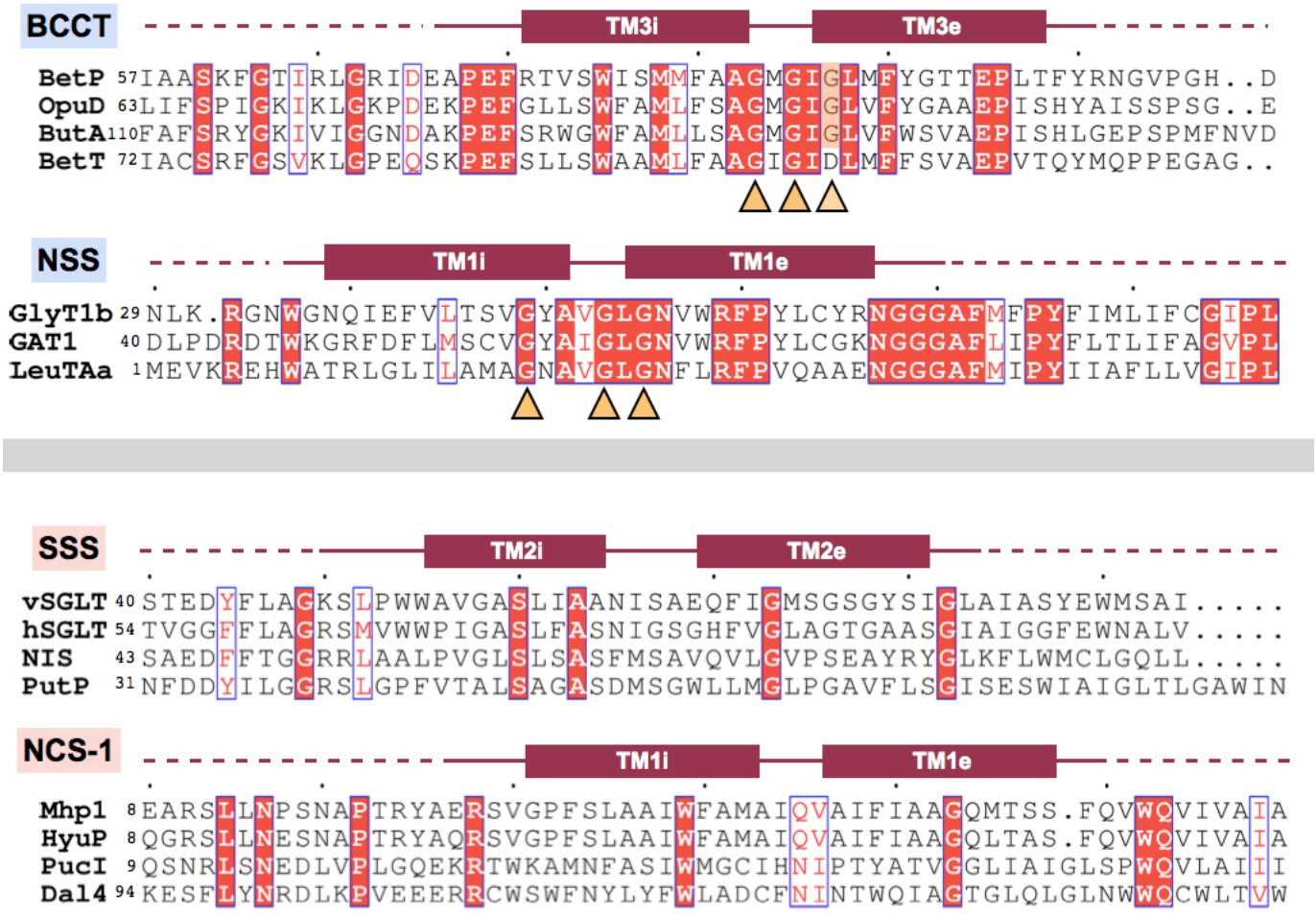

Figure S6: Sequence alignments of the first helix of the first repeat of different transporters of the BCCT, NSS, SSS and NCS-1 family by ClustalW multiple sequence alignment displayed by ESPript 2.2 (http://espript.ibcp.fr/ESPript). Conserved glycines are indicated by orange triangles.

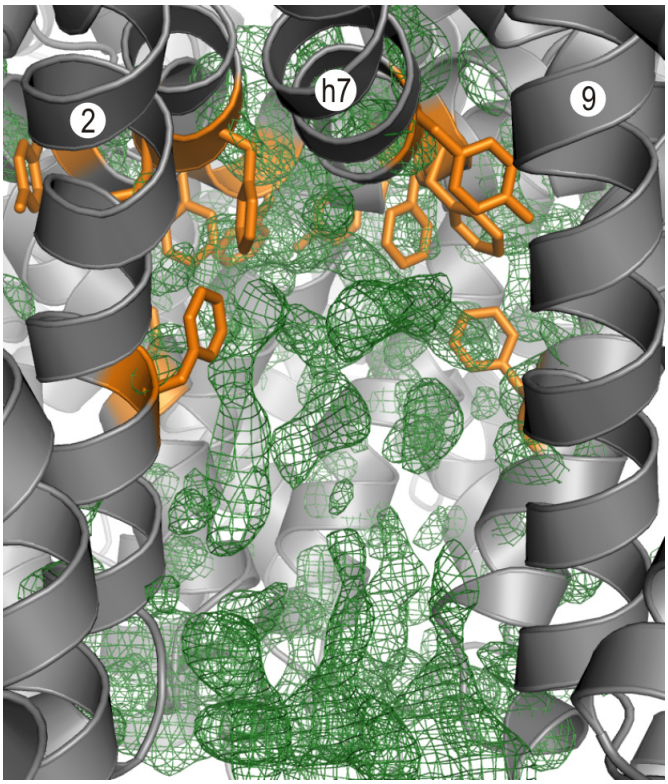

Figure S7: Central cavity of the BetP trimer. Aromatic side chains of helix 7 and TM2 point into unmodelled Fo-Fc density (shown in green at 1.8σ), representing bound lipid or detergent.

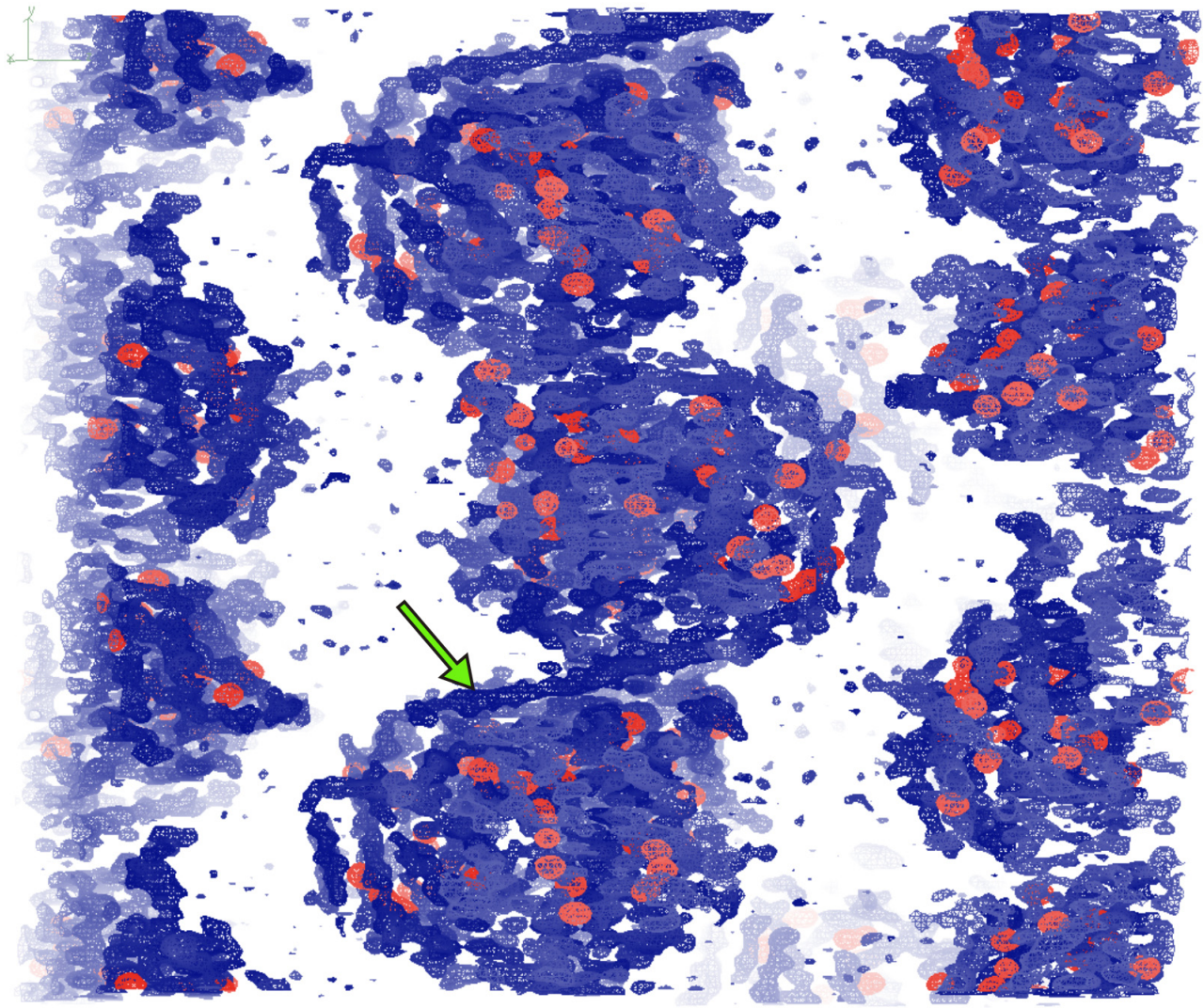

Figure S8: Electron density shown in blue at 1.3σ after solvent flattening with SOLOMON[6] in SHARP/autoSHARP[5]. The electron density represents the initial map after SAD phasing, hence it is not averaged using the NCS nor corrected for anisotropy nor any negative B-factor is applied. The anomalous difference map for the selenium sites is shown in red at 3.5σ. The arrow points towards the C-terminal domain making the crystal contact to the adjacent trimer.

Table 1 | Data collection, phasing and refinement statistics

	Se-BetPΔN29	
Data collection		
Space group	$P2_12_12_1$	
Cell dimensions		
a, *b*, *c* (Å)	118.09, 129.42, 182.94	
α, β, γ (º)	90, 90, 90	
	Peak	
Wavelength	0.9794	
Resolution (Å)	39.47 – 3.35 (3.55-3.35)	
R_{merge}	9.9	(64.8)
$I/\sigma I$	23.2	(1.0)
Completeness (%)	90.7	(44.1)
Redundancy	18.9	(1.7)
Refinement		
Resolution (Å)	39.47 – 3.35 (3.55-3.35)	
No. reflections	37151	(2967)
R_{work}/ R_{free}	25.68/26.49 (24.12/23.95)	
No. atoms	11737	
Protein	11353	
Ligand/ion	384	
Water	-	
B-factors	64.34	
Protein	-	
Ligand/ion	-	
Water	-	
R.m.s deviations		
Bond lengths (Å)	0.002	
Bond angles (º)	0.34	

Table 2 | Structure comparison with DaliLite[16]

Structure comparison		RMSD (Å)
BetP repeat 1	BetP repeat 2	3.5
LeuT repeat 1	LeuT repeat 2	5.2
SGLT repeat 1	SGLT repeat 2	4.3
Mhp1 repeat 1	Mhp1 repeat 2	4.3
Scaffold		
BetP scaffold	LeuT scaffold	3.7
BetP scaffold	SGLT scaffold	3.9
BetP scaffold	Mhp1 scaffold	3.8
LeuT scaffold	SGLT scaffold	3.5
SGLT scaffold	Mhp1 scaffold	3.4
Mhp1 scaffold	LeuT scaffold	2.5
BetP TM10-TM12	LeuT TM8-TM10	3.1
BetP TM10-TM12	SGLT TM9-TM11	3.8
4-helix bundle		
BetP 4-helix bundle	LeuT 4-helix bundle	3.2
BetP 4-helix bundle	SGLT 4-helix bundle	3.1
BetP 4-helix bundle	Mhp1 4-helix bundle	3.4
LeuT 4-helix bundle	SGLT 4-helix bundle	3.5
SGLT 4-helix bundle	Mhp1 4-helix bundle	3.6
Mhp1 4-helix bundle	LeuT 4-helix bundle	3.2
Scaffold comparison used for superposition in Fig.4		
BetP TM6-7 TM11-12	LeuT TM4-5 TM9-10	2.9
BetP TM6-7 TM11-12	SGLT TM5-6 TM10-11	2.5

References

1. Schiller, D., Krämer, R. & Morbach, S. Cation specificity of osmosensing by the betaine carrier BetP of *Corynebacterium glutamicum*. *FEBS Lett.* **563,** 108-112 (2004).
2. Kabsch, W. *J. Appl. Cryst.* **26,** 795-800 (1993).
3. Evans, P. Scaling and assessment of data quality *Acta Crystallogr.* **D62,** 72-82 (2006).
4. Sheldrick, G.M. A short history of SHELX. *Acta Crystallogr.* **A64,** 112-122 (2008).
5. Vonrhein, C., Blanc, E., Roversi, P. & Bricogne, G. Automated structure solution with autoSHARP. *Methods Mol. Biol.* **364,** 215-230 (2007).
6. Abrahams, J.P. & Leslie, A.G.W. Methods used in the structure determination of bovine mitochondrial F_1 ATPase. *Acta Crystallogr.* **D52,** 30-42 (1996).
7. Cowtan, K. DM: An automated procedure for phase improvement by density modification. *Joint CCP4 and ESF-EACBM Newsletter on Protein Crystallography* **31,** 34-38 (1994).
8. Emsley, P. & Cowtan, K. Coot: model-building tools for molecular graphics. *Acta Crystallogr.* **D60,** 2126-2132 (2004).
9. Jones, T.A., Zou, J.-Y., Cowan, S.W. & Kjeldgaard, M. Improved methods for the building of protein models in electron density maps and the location of errors in these models. *Acta Crystallogr.* **A47,** 110-119 (1991).
10. Blanc, E. *et al.* Refinement of severely incomplete structures with maximum likelihood in BUSTER-TNT. *Acta Crystallogr.* **D60,** 2210-2221 (2004).
11. Terwilliger, T.C. *et al.* Iterative model building, structure refinement and density modification with the PHENIX AutoBuild wizard. *Acta Crystallogr.* **D64,** 61-69 (2008).

12. Simon C. Lovell, I.W.D., W. Bryan Arendall III, Paul I. W. de Bakker, J. Michael Word, Michael G. Prisant, Jane S. Richardson, David C. Richardson Structure validation by C-alpha geometry: phi, psi, and C-beta deviation. *Proteins: Structure, Function, and Genetics* **50,** 13 (2003).

13. Kappes, R.M., Kempf, B. & E., B. Three transport systems for the osmoprotectant glycine betaine operate in Bacillus subtilis: characterization of OpuD. *J. Bacteriol.* **178,** 5071-5079 (1996).

14. Schiller, D., Rübenhagen, R., Krämer, R. & Morbach, S. The C-terminal domain of the betaine carrier BetP of *Corynebacterium glutamicum* is directly involved in sensing K^+ as an osmotic stimulus. *Biochemistry* **43,** 5583-5591 (2004).

15. Schiefner, A. *et al.* Cation-π interactions as determinants for binding of the compatible solutes glycine betaine and proline betaine by the periplasmic ligand-binding protein ProX from *Escherichia coli*. *J. Biol. Chem.* **279,** 5588-5596 (2004).

16. Holm L., P.J. DaliLite workbench for protein structure comparison. *Bioinformatics* **16,** 566-567 (2000).